

The potential of satellite remote sensing for monitoring the onset of volcanic activity on Taipei's doorstep

Hai-Po Chan, Chung-Pai Chang, Tang-Huang Lin, Matthew Blackett, Hao Kuo-Chen & Andrew Tien-Shun Lin

To cite this article: Hai-Po Chan, Chung-Pai Chang, Tang-Huang Lin, Matthew Blackett, Hao Kuo-Chen & Andrew Tien-Shun Lin (2019): The potential of satellite remote sensing for monitoring the onset of volcanic activity on Taipei's doorstep, International Journal of Remote Sensing, DOI: [10.1080/01431161.2019.1667549](https://doi.org/10.1080/01431161.2019.1667549)

To link to this article: <https://doi.org/10.1080/01431161.2019.1667549>



Published online: 17 Sep 2019.



Submit your article to this journal [↗](#)




View related articles [↗](#)



View Crossmark data [↗](#)



The potential of satellite remote sensing for monitoring the onset of volcanic activity on Taipei's doorstep

Hai-Po Chan ^a, Chung-Pai Chang^{a,b}, Tang-Huang Lin^a, Matthew Blackett^c, Hao Kuo-Chen^b and Andrew Tien-Shun Lin^b

^aCenter for Space and Remote Sensing Research, National Central University, Jhongli, Taiwan; ^bDepartment of Earth Sciences, National Central University, Jhongli, Taiwan; ^cSchool of Energy, Construction & Environment, Coventry University, Coventry, UK

ABSTRACT

The Tatun Volcanic Group (TVG) in northern Taiwan is the sole volcanic region on the island, with its last eruptive episode around 5,500 years ago. It has been suggested that the TVG retains the capacity for volcanic explosivity which has the potential to devastate the nearby Taipei metropolitan area of 7 million inhabitants. Though the probability of future eruption is low by probabilistic estimation, the vulnerability to volcanic hazards is high for Taipei given that it is the centre of population, industry, and government for the island. An assessment of any activity precursors is thus vital but also particularly challenging. Here, we perform an eruption-potential assessment based on the analysis of a sixteen-year Land Surface Temperature (LST) time series of data derived from satellite-retrieved thermal imagery. A Hilbert-Huang Transform (HHT) is applied to decompose oscillatory components of various time-scales within the LST time series. The annual-period components are compared with those from two active volcanoes in the Philippines to assess the potential for eruption cycles in the TVG. Results from the Philippine volcanoes show that annual-period components of LST tend to lose their regularity following an eruption. By contrast, the regular annual-period component of LST of the TVG Taiwan suggests a quiet and resting status with no sign of an imminent eruption.

ARTICLE HISTORY

Received 19 February 2019
Accepted 22 July 2019

1. Introduction

Volcanoes are dangerous, for numerous geologic and hydrologic hazards may result from a volcanic eruption, often simultaneously. An assessment of any volcanic activity precursors is thus vital but also particularly challenging. However, remote-sensing technology has dramatically improved our capacity to explore, monitor and measure volcanic activities for the past 50 years (Queißer, Burton, and Kazahaya 2018; Blackett 2017; Ramsey, Harris, and Crown 2016; Carn, Clarisse, and Prata 2016; Ramsey and Harris 2013; Steffke and Harris 2011). Applications of satellite remote-sensing observations have transformed our ability to monitor volcanic eruptions, these techniques provide

long-term monitoring data on the pending volcanoes for better understanding how volcanoes work; and enable us to compare behaviours of various volcanoes in ways not feasible from on-site or ground-based observations (Pyle, Mather, and Biggs 2013; Wooster et al. 2013; Gupta 2017; Hellman and Ramsey 2004; Spinetti et al. 2008; Kereszturi et al. 2018; Pieri and Abrams 2004).

Observations in the thermal-infrared region (3–35 μm) of electromagnetic (EM) wave are used to detect volcanic activity which often relates directly to the heat transfer from the Earth interior to the surface. Based on the physics of thermal infrared radiation, satellite remote-sensing techniques have been extensively applied for detecting and monitoring volcanic activity worldwide and present propitious results (Wright et al. 2002; Flynn, Harris, and Wright 2001; Delle Donne et al. 2010; Ewert, Guffanti, and Murray 2005; Webley et al. 2008; Bull et al. 2012; Blackett 2013; Blackett 2015; Roberti et al. 2018). Among these applications, thermal signatures can be detected in the volcanic activity. Thermal signatures include volcanic eruption and volcanic unrest, such as a fresh lava flow, an active lava lake, or even more subtle, a degassing surface and a heated crater lake. Regularly obtained remote-sensing data in the volcanic area are thus essential in understanding the volcano's current status as well as future potential activities. In addition, it is clearly advantageous to make such observations remotely and at a safe distance (Blackett 2017).

The Tatun Volcanic Group (TVG) is proven to be an active volcano based on the seismic wave analysis. A body of geochemical and seismological studies has shown that a magma source exists beneath the TVG and that future eruptions are possible (Yang, Sano, and Song 1999; Kim et al. 2005; Konstantinou, Lin, and Liang 2007; Konstantinou et al. 2009; Tsai et al. 2010; Belousov et al. 2010; Lin 2016; Nurmawati and Konstantinou 2018). The magma source has been estimated to be about a quarter size of Taipei City, with estimated dimensions of 15 km in length and 6 km in width; a thickness (height) of 3.9–10.4 km and an overall volume of 350–936 km^3 upon magma reservoir's level of partial melting (Lin 2016).

The TVG is on Taipei's doorstep, just 15 km north and overlooking the metropolitan region of approximately 7 million. Such proximity is comparable to what is arguably the world's most dangerous volcano: Vesuvius, which is merely 12 km from downtown Naples. The TVG has no documented evidence of eruptions but was formed by multiple Quaternary volcanic eruptions into the late Tertiary sedimentary basement. Today, the TVG consists of 23 well-preserved volcanic edifices composed mainly of lava rocks, and pyroclastic deposits. Mt. Qixing, Mt. Dajianhou, and Mt. Huangzuei among them are young volcanoes (0.3–0.2 Ma) (Song et al. 2007; Song, Tsao, and Lo 2000). TVG consists of E-W and SW-NE volcanic ridges between the Jinshan and Kanchiao faults (Figure 1). The length of each ridge is approx. 15 km they reach an elevation of 800–1,000 m asl. The SW-NE ridge is steeper and older than the E-W ridge. Numerous volcanic features such as craters, cones, lava flows, and pressure ridges are well preserved in E-W ridge (Yang et al. 2004).

Seismological and structural geological studies show prominent extensional tectonism in the TVG (Song, Tsao, and Lo 2000; Jyr-Ching et al. 1996; Chu, Lee, and Teng 1998a). A group of minor faults in the TVG has been delineated based on the comprehensive map of lineaments extracted from a digital terrain model, aerial photographs, and field validations. The minor faults zone (around 3.5 km in width by 16 km in length) is distributed in a NE-SW trend and is largely parallel to the Jinshan fault. Tectonic fractures and hydro-thermal activities are prevalent throughout the zone (Chu, Lee, and Teng 1998a).

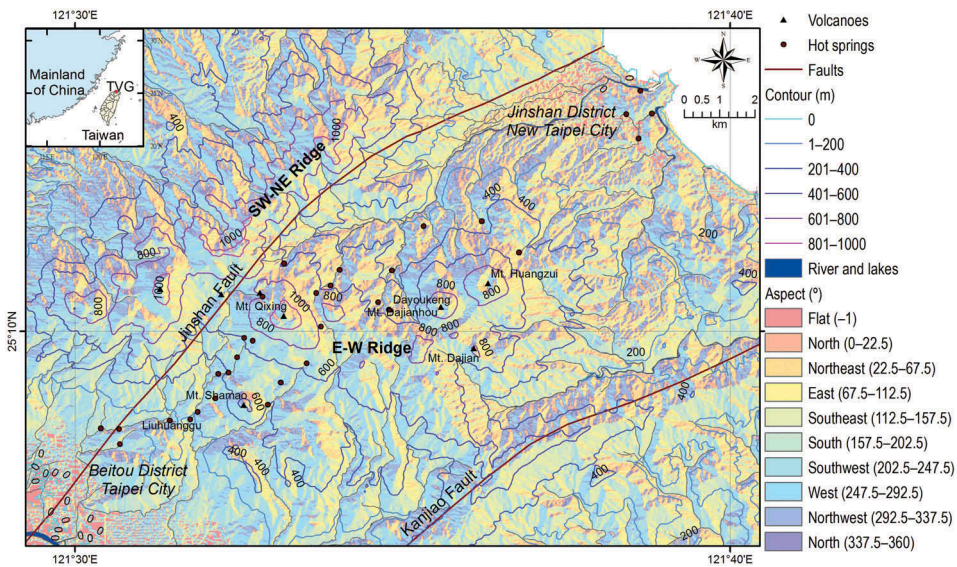


Figure 1. Geography, aspect and contour line map of TVG, northern Taiwan. Main volcanic ridges, volcanoes, and hot springs have been indicated.

Magma source usually contains near-vertical faults through impermeable intrusions, meaning that heat is transferred from the geothermal system to the surface and that associated thermal anomalies can be detected via surface manifestations, thermal infrared mapping, geochemical analyses or exploration drillings (Cheng 1979; Zhao, Hobbs, and Ord 2008). The TVG is no exception to these features with the Jinshan fault in particular, being the primary fault of the TVG related to volcanic and hydrothermal activities and the most widely investigated (Chang et al. 2010; Wang et al. 2010; Wang 2008; Teng et al. 2001; Chu, Lee, and Teng 1998b). Based on previous investigations, the Jinshan fault zone in the TVG is the most likely heat channel of the magma source and effectively serves as the observing window (i.e. polygonal region of Jinshan fault in Figure 3). Variations in Land Surface Temperature (LST) throughout this fault zone are indicative of volcanic activity at depth.

In short, the TVG is active and has an eruptive potential based on previous studies. In addition to the 7 million people who live in the vicinity, there are two nuclear power plants within 15 km of the volcano group, thus necessitating an urgent need for in-depth investigation. Past studies on the TVG aforementioned have generally focused on geochemical and seismological observations. Volcanic eruption forecasting is an interdisciplinary monitoring and research effort to predict the time and severity of a volcano's eruption. Taiwan Volcano Observatory at Tatun (TVO) has been established for this aim since 2011. It involves volcano seismology, gas emissions, ground deformation, and on-site thermal monitoring, but no remote-sensing thermal monitoring system has been applied. Our study, however, utilizes satellite Thermal Infrared (TIR) remote sensing to the monitoring of this active volcanic region, focusing on its future eruptive potential. This volcano at Taipei vicinity apparently has woken up the people of northern Taiwan to the risks posed by. For instance, a shallow (6.4 km depth), magnitude-4 earthquake in February 2014 within TVG limits has set alarm bells ringing for it was the biggest volcanic event in 26 years.

2. Materials and methods

Both 30-m (spatial resolution) Landsat imagery and 1-km Moderate Resolution Imaging Spectroradiometer (MODIS) LST products are used in this study. Landsat and MODIS imagery are complementary to each other in terms of imagery spatial and temporal resolutions. Landsat imagery has the higher spatial resolution (30-m) but lower temporal resolution (16-day revisit), in contrast, MODIS LST products have the higher temporal resolution (sub-daily) but lower spatial resolution (1-km). MODIS LST products are ready for further analyses, while Landsat data are required for post-processing to obtain the LST. The main study area is TVG volcano, Taiwan. However, for a comparative study with active volcanoes of the same tectonic region. Mayon volcano and Canlaon volcano of Philippines are also included in the analysis. Thus, satellite thermal infrared imagery at TVG volcano, Taiwan and Mayon volcano; Canlaon volcano, Philippines for the period July 2002–June 2018 are selected based on the image quality of cloud coverage in USGS imagery archives. The flow chart on specific procedures of this study are illustrated in [Figure 2](#).

2.1. LST retrieved from Landsat 7 imagery

The physics of LST retrieval from infrared imagery is the Planck Function, and this has been applied to the Landsat ETM+ data to estimate the Brightness Temperature (BT) of the surface. This was then converted to a value of LST by incorporating associated values of surface emissivity, as derived from the Landsat 7+ Normalized Difference Vegetation Index (NDVI) data. The detailed data processing procedures and result validation have been documented in the previous work (Chan, Chang, and Dao 2018; Chan and Chang 2018).

There are no overtly active craters in the TVG for LST monitoring and the main thermal emissions, therefore, are from fumaroles and hot springs scattered throughout the group (see [Figure 1](#)). Unfortunately, these sites are not concentrated and the magnitudes of emission are subtle, thereby meaning that sensors with a high temporal resolution but low spatial resolution (e.g. MODIS) are unsuitable for monitoring thermal activity at the TVG. The higher spatial resolution of the Landsat 7 Enhanced Thematic Mapper Plus (ETM+) thermal infrared imagery (60-m, resampled to 30-m pixels) however, is ideal and is used to delineate the thermal anomaly pattern on the ground. [Figure 3](#) illustrates the LST distribution of TVG from Landsat 7 ETM+ band 6 data on 3 December 2001 (Scene ID: LE07_L1TP_117043_20011203_20170202_01_T1) and 12 December 2016 (Scene ID: LE07_L1TP_117043_20161212_20170201_01_T1), respectively. Specified polygonal region of interest (ROI) of Jinshan fault chosen as the representative zone for the further monitoring analysis is displayed. Despite a sixteen-year gap between these images, little has changed in terms of the LST distributions. Both scenes, for example, indicate an LST range of 15–34°C. Thermally anomalous regions at the TVG's E-W and SW-NE volcanic ridges (enclosed in the outlined square in [Figure 3](#)) are generally 3–6°C higher than the surroundings. Thermal anomaly patterns are in line with the occurrence of hot springs which are indicated by the solid dots. The LST at the E-W ridge is higher than the SW-NE ridge. Furthermore, spatial distributions of higher LSTs overlap with the Jinshan fault TVG as highlighted in the polygonal Region of Interest (ROI) in [Figure 3](#). Since fault zones are the common pathways for the emanation of subsurface heat in volcanic areas, the Jinshan fault zone ROI is considered as the representative zone for monitoring the TVG analysis.

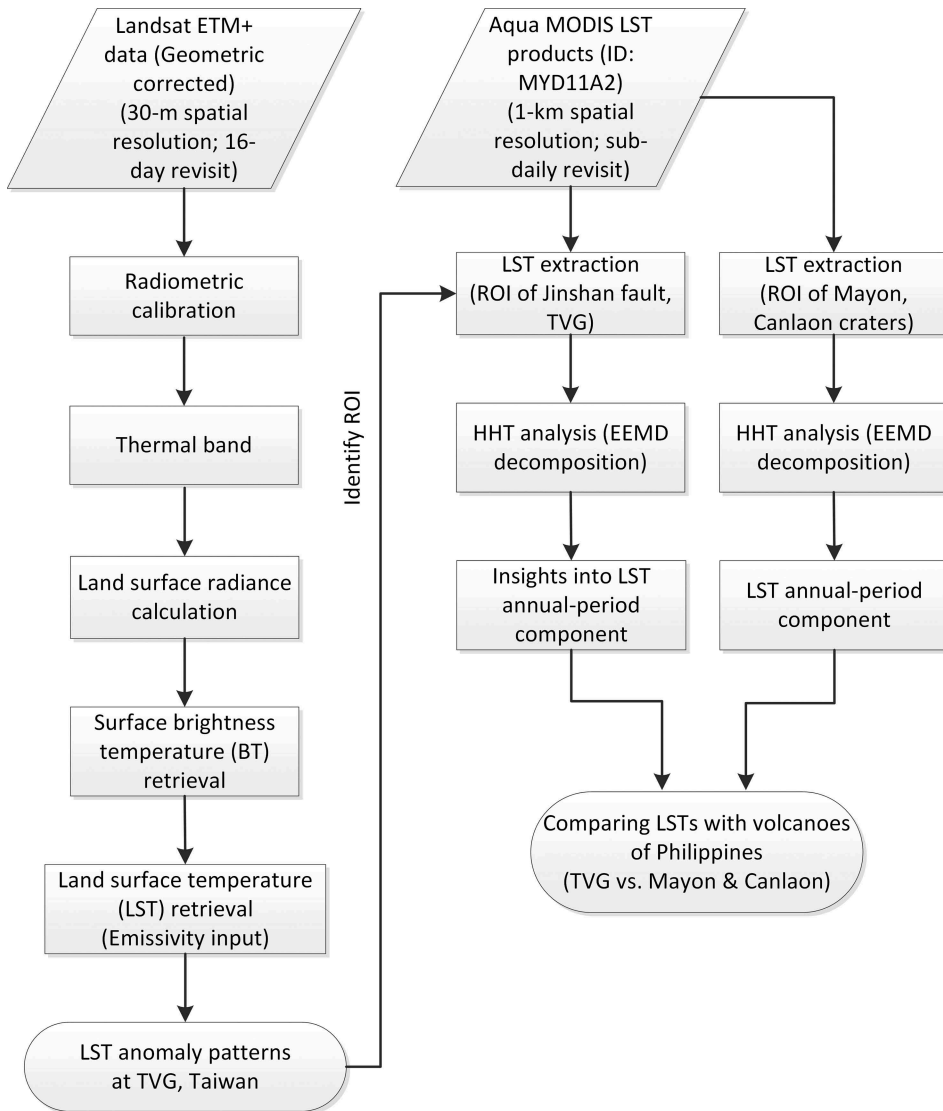


Figure 2. Flow chart of the procedures conducted in this study.

2.2. MODIS 8-day average LST products

Landsat 7 imagery has the benefit of a higher spatial resolution (60-m) but is less appropriate for LST monitoring due to its 16-day revisit period. MODIS, in contrast, supplies sub-daily imagery at a 1-km spatial resolution and while such a resolution is imperfect, it is acceptable for our purposes of monitoring. MODIS 8-day LST night-time data (Product ID: MYD11A2) from 2002–2018 at TVG was analysed, focusing on the Jinshan fault zone which has been chosen for a representative monitoring area of TVG. The MYD11A2 product provides 8-day average per-pixel LST. Each pixel value is the simple average of all the corresponding daily LST pixels within that 8-day period. An eight-day compositing period was selected because twice that period (16-day) is the exact ground track repeat period of the Aqua platform. The daily LST

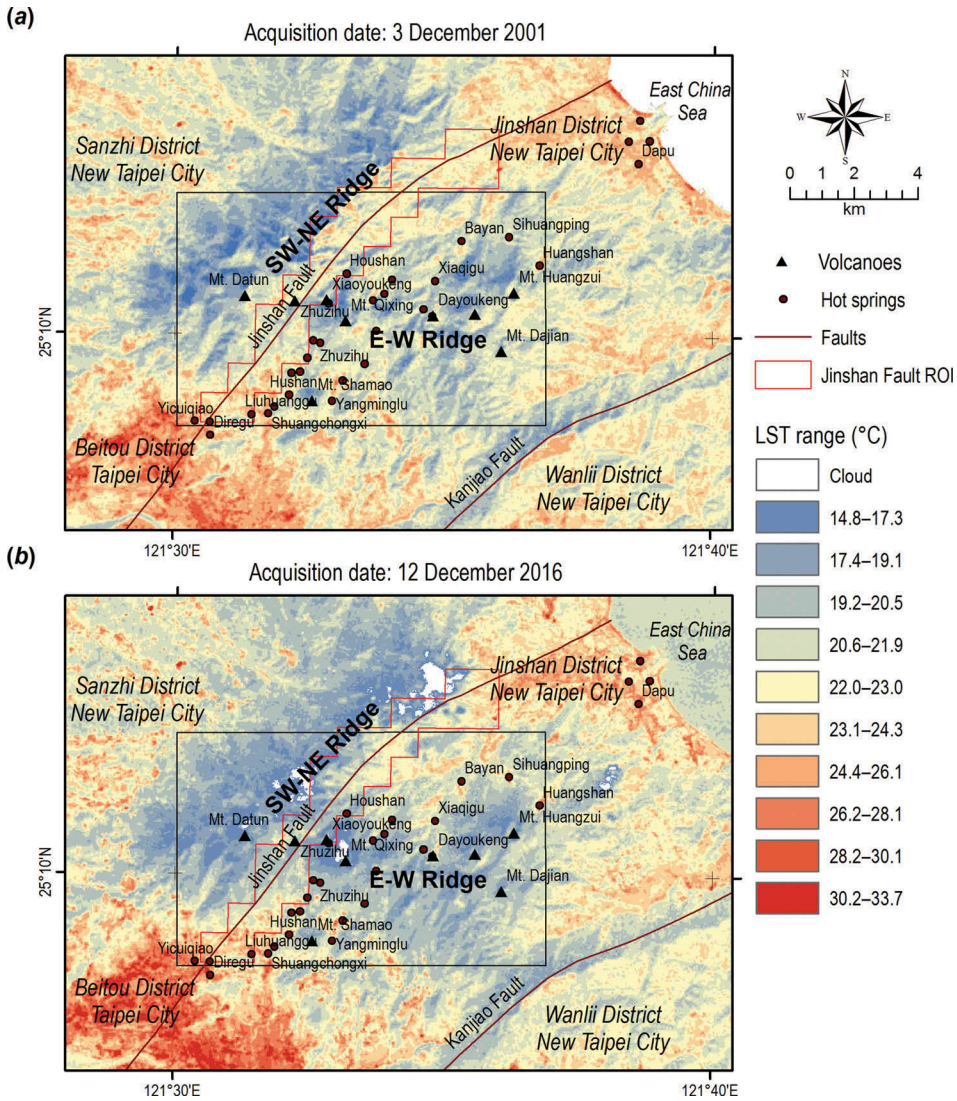


Figure 3. Pattern of LST distribution in TVG from Landsat 7 ETM+ imagery on (a) 3 December 2001 and (b) 12 December 2016, respectively. The outlined square is the focused area which is less contaminated by the anthropogenic activity from urban area. Thermal anomalous areas (polygonal region of interest of Jinshan fault) are illustrated by red colour polygon in the imagery. The thermal anomaly at ROI of Jinshan fault is persistent in 2001 and 2016. Note that the imagery on 12 December 2016 is contaminated by some cloud.

product is derived from the night LST algorithm (Wan and Zhao-Liang 1997; Wan 2014) based on pairs of night-time observations in seven MODIS TIR bands (bands 20, 22, 23, 29, and 31–33; wavelength 3.6–12.3 μm). According to the general accuracy statement from MODIS land team of National Aeronautics and Space Administration (NASA), the Aqua MODIS (Product ID: MYD11) Collection 5 (C5) products have accuracy better than 1K (0.5 K in most cases), as expected pre-launch of the sensor. The MODIS LST imagery on each volcanic zone (TVG, Mayon and Canlaon) to visually assess the reliability of a 1 km by 1 km pixel resolution is

illustrated in [Figure 4](#). The 8-day LST product was selected to reduce the occurrence of cloud-cover within the LST imagery which would reduce the reliability of the dataset extracted. The availability of an 8-day product is a significant advantage over the data from Landsat 7 which, being available only every 16 days, is regularly contaminated by cloud. [Figure 5](#) (the blue line) illustrates the night-time MODIS 8-day average LST of Jinshan fault zone in TVG (i.e. based on the polygonal ROI in [Figure 3](#)) for 2002–2018.

Given that the MODIS LST dataset of 2002–2018 contains a vast wealth of information, specialized techniques are required to identify and process any signals within it. Given the nonlinear and nonstationary nature of the LST time series, the Hilbert-Huang Transform (HHT) was chosen for this process to decompose the LST dataset into its temporal and frequency domains. The goal of HHT in this study is to break down MODIS LST time series into various monochrome components in time-domain. HHT is the time-frequency transform method for a nonlinear and nonstationary dataset (Huang et al. 1998; Nunes and Eric 2009; Huang et al. 2009). Compared with Fourier or Wavelet transforms, HHT is an empirical algorithm that provides more desirable time-domain and frequency-domain resolution of the transformed data set. HHT's key advantage is Ensemble Empirical Mode Decomposition (EEMD) with which a complicated dataset can be transformed into a smaller number of intrinsic mode functions (IMFs). Each IMF is often related to a particular physical process. The resulting decompositions (i.e. IMFs) make a nearly complete and orthogonal basis for the original dataset. This decomposition method is a data-driven, adaptive approach and with high efficiency (Huang and Zhaohua 2008; Wang et al. 2014)

The HHT's key empirical algorithm, the EEMD, was applied to obtain an accurate expression of MODIS LST in the time-frequency-energy (amplitude) domain. The MODIS LST 8-day average data and the corresponding EEMD are shown in [Figure 5](#).

The timescale of each EEMD component is important for it implies not only the period of a particular physical process but also information for the potential assessment of volcanic unrest or eruption in TVG. Depended on the extent of LST data available, we are only allowed to confine the onset prediction to the immediate future (i.e. to the decadal timescale). To identify the spectrum peak for determining the dominant frequency of each component of MODIS LST, a Fourier transform has been applied to derive the dominant period for each EEMD component in [Figure 5](#). The calculated dominant period of LST and EEMD components C1–C8 are as follows: LST is 363.3 days (around one year); C1 is 23.3 days (around a month); C2 is 75.5 days (around two month); C3 is 123.7 days (one-third year); C4 is 363.3 days (around one year); C5 is 968.9 days (around two and a half year); C6 is 1,937.7 days (around half a decade); C7 is 5,813 days (around a decade and a half); C8 is 5,813 days (around a decade and a half).

All the EEMD components of the MODIS LST dataset form nearly the complete LST time series. These eight components (C1–C8) have been extracted by HHT from around 700 data points of MODIS LST dataset in the Jinshan fault thermal anomalous areas. They are the representative set that captures the most information from the original LST. And each EEMD component is connecting with the certain physical process either surficial or underneath. For instance, component C4 has 370-day (annual) period which is the same with the dominant period of original LST. And the annual-cycle of original LST is caused by the sunlight, season and vegetation. C1 and C2 of alike amplitudes have a period about three weeks and two months, respectively. Both are superimposed with irregular spikes on random oscillations. C3 has a period of one-third year and a lower amplitude which may

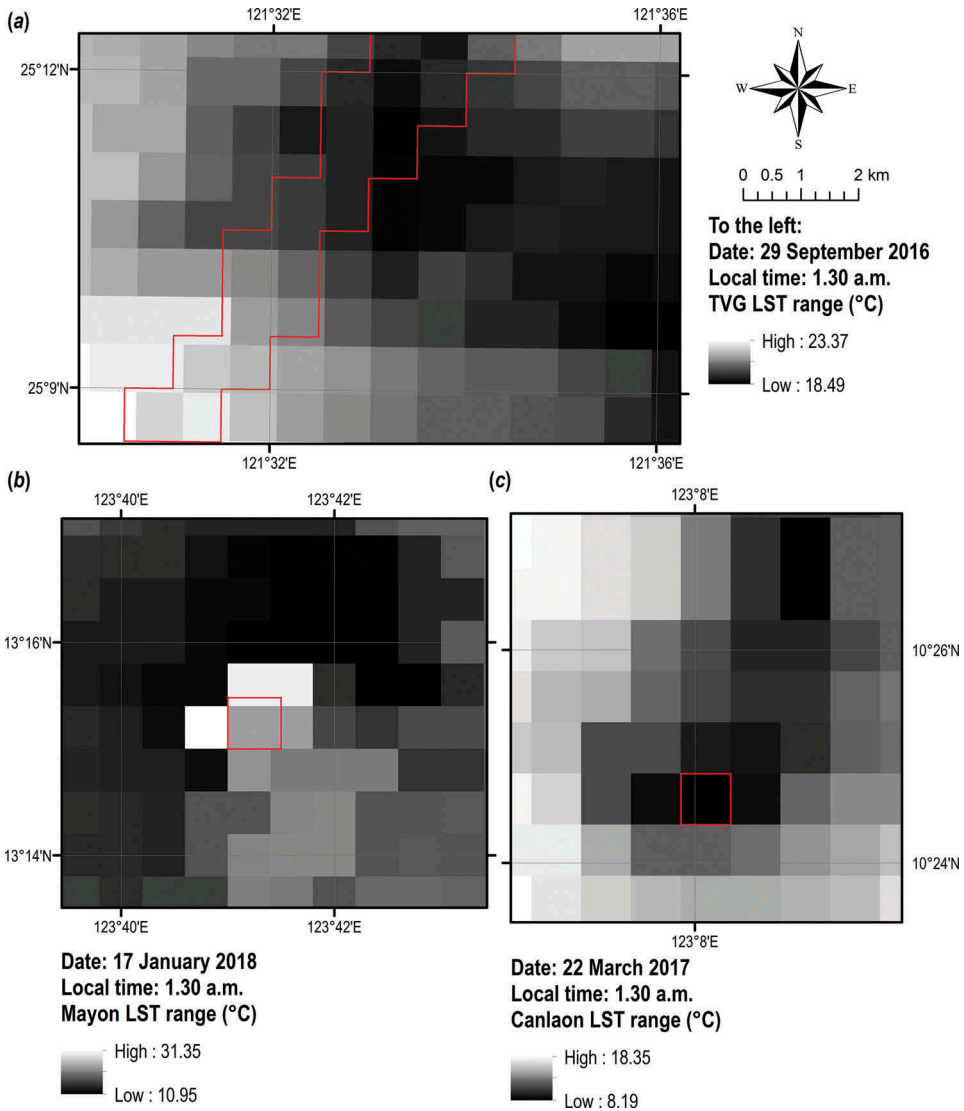


Figure 4. The exemplary MODIS LST imagery (Product ID: MYD11A2) with 1 km by 1 km pixel resolution on each volcanic zone. Thermal anomalous areas of TVG (multiple pixels for Jinshan fault area) and volcano craters of Mayon and Canlaon (one pixel for each crater area) are illustrated by red colour polygonal region in each imagery. To allow for a better comparison of crater LSTs, imagery date chosen for Mayon volcano is during its eruption in 2018, while for Canlaon volcano is not. (a) TVG of Taiwan. (b) Mayon and (c) Canlaon of Philippines.

be related to the atmospheric circulation. C5–C8 have amplitudes 1 order lower than others. C5 and C6 are of inter-annual timescales. C5 is of quasi-biannual, and C6 has the period about half a decade. C7 and C8 have periods in decadal timescales. C7 has a period of one and half decade, and C8’s period is a few decades and longer. The upward-going LST trend of the bottom plot appears very gentle variation from 2002–2018 (Chan and Chang 2018).

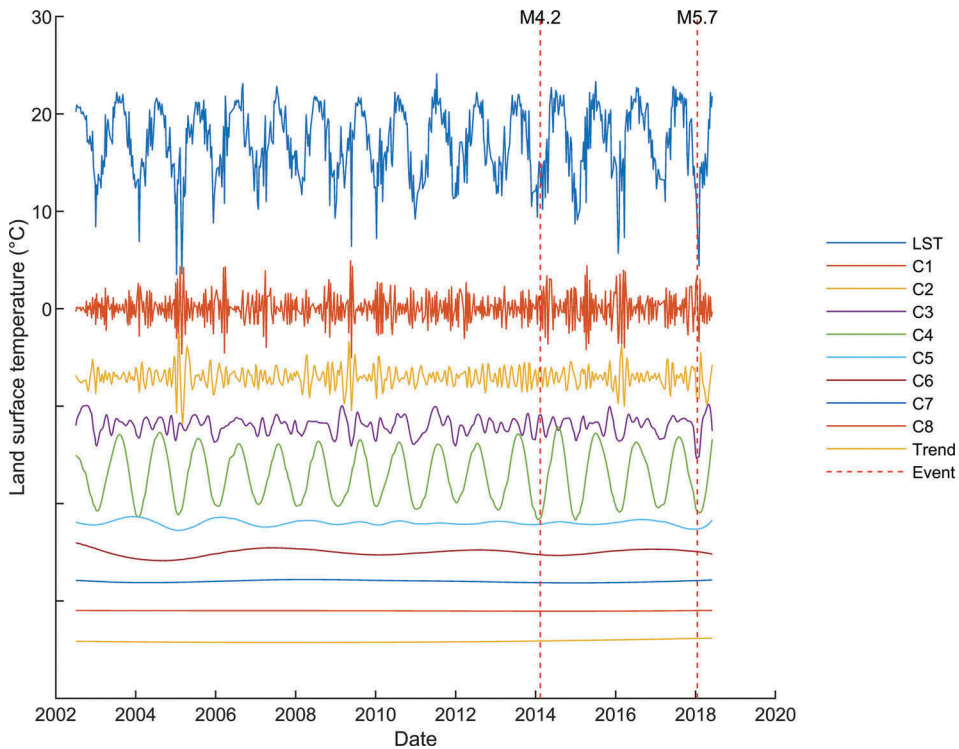


Figure 5. HHT decomposition of the MODIS LST dataset from July 2002–June 2018 for TVG's Jinshan fault zone (Chan and Chang 2018). The original MODIS LST is represented by the upper blue line while C1–C8, HHT decomposed components are plotted beneath. The vertical dashed red line indicates the recorded earthquake events >M4 on 12 February 2014 (ML = 4.21, 6.4 km deep) and 17 January 2018 (ML = 5.7, 140 km deep).

3. Results and discussion

3.1. Insights into LST annual-period component

LST is the radiative temperature of the ground. It can be contributed to by heat sources both from above and beneath the land surface. In this study, geothermal or volcanic sources are assumed to be the chief heat suppliers below, while insolation and air temperature are the contributors above. Seasonal LST components correlate with the LST component C4, while the irregular patterns are geothermal and/or volcanic in source. The data shows that the geothermal contribution is rather consistent on a multi-decadal to millennial-scale but any volcanic contribution (i.e. eruption or volcanic unrest) would not be consistent and would disturb the regular patterns. Based on the above reasoning, we anticipate that investigation on the annual-period component C4 (period of 370 days; around one year) is feasible to the potential onset assessment of TVG.

For detailed investigation on the C4 component, HHT decomposition of LST has been compared with the near-surface on-site air temperature. The on-site monthly air temperature has been detrended to serve as a reference for the surface meteorology annual cycle. The annual-period component of TVG's LST and the regular annual-cycle air temperature is shown in Figure 6. Statistics parameters Kurtosis and Skewness as

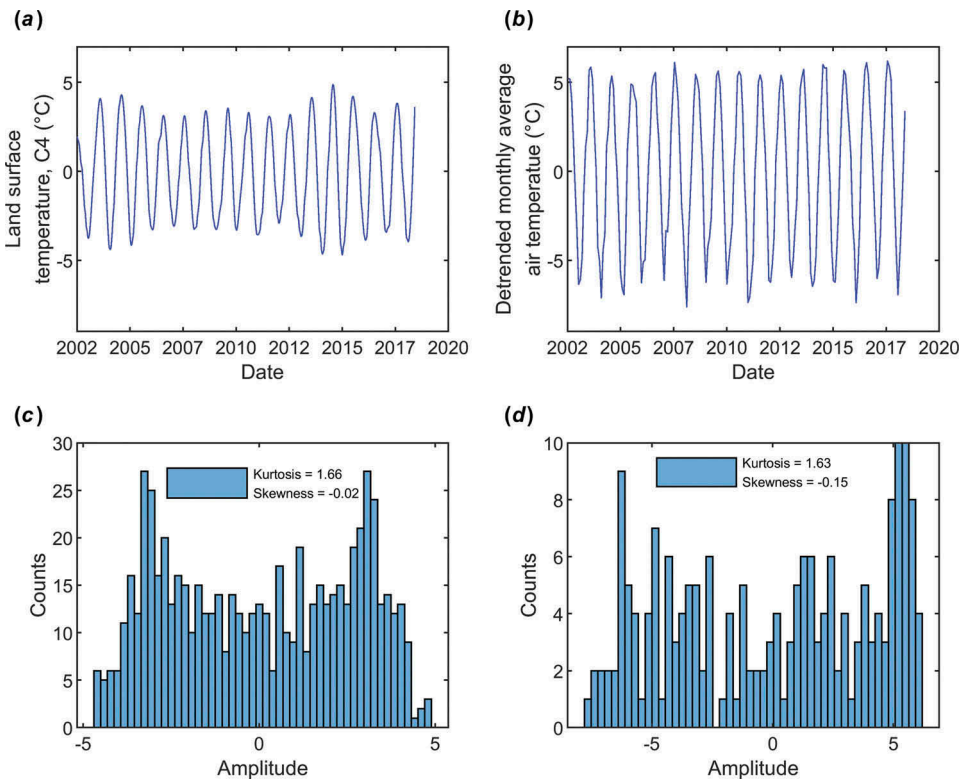


Figure 6. Annual-period component of LST vs. the regular annual-cycle air temperature in TVG. (a) and (c) show the decomposed LST component 4 (C4; annual-period component) and its corresponding histogram. (b) and (d) are the detrended monthly air temperature and the corresponding histogram. The air temperature has been served as the reference for comparison.

numerical measures of the shape have been calculated for quantifying the similarity level between the time series. The high resemblance of these two indicates that the LST reliably recorded the climate annual cycles as its annual component. The higher the level of similarity often implies the lower the disturbance from other factors such as volcanic heating. In contrast, the distortion of TVG's LST annual-period component would indicate the heat influence caused by the volcanic eruptive or related earthquake events. Figure 7 illustrates the comparison in a more comprehensive manner.

3.2. Comparing LSTs with volcanoes of Philippines

True physical processes underneath the EEMD components (C1–C8) are quests to reveal for assessing the eruption potential of TVG. They are generally hard to obtain owing to the unknown natural complexity of volcanic systems. However, the alternative way to understand the eruption potential of TVG is comparing with the current active volcanoes around the world. For better understanding TVG's eruption potential, we compare its data with that of a persistently active volcanic region. Given the geological and climatic similarity of Taiwan and the Philippines, active volcanoes of the Philippines were chosen: Mayon volcano (Stratovolcano with an elevation of 2,462 m) and Canlaon volcano (Stratovolcano with an

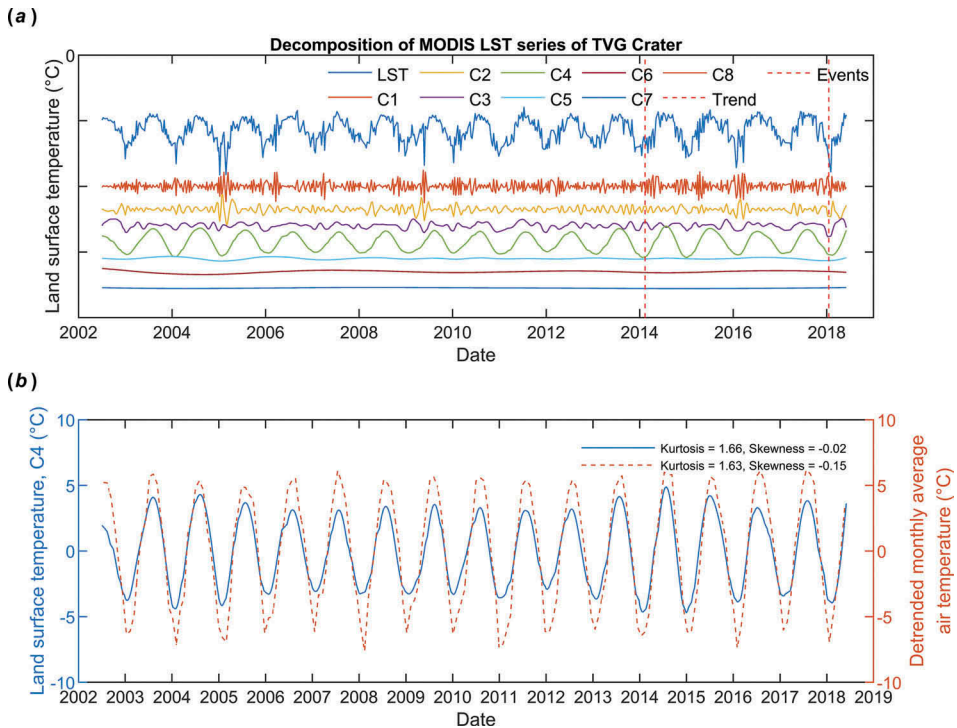


Figure 7. Decomposition of the MODIS LST at TVG. (a) EEMD decomposed MODIS LST of TVG from 2000–2019. The original MODIS LST is on the top plot, followed by the decomposed components C1–C8, and the trend is on the bottom plot. Recorded earthquakes are indicated by dashed vertical red lines. (b) Comparison between the decomposed annual-cycle LST component 4 (C4) and the detrended monthly air temperature at TVG.

elevation of 2,435 m). Both Taiwan and Philippines are formed by the collision of Philippine Sea plate and Eurasia plate. The volcanoes are the tectonic products of the convergence of plate boundaries. i.e. the shallow west-dipping subduction of the Philippine Sea plate at the Philippine Trench produces a line of volcanoes associated with a back-arc basin in the east front of Eurasia plate (Divis 1980). Figure 8 illustrates the tectonic setting in the Philippine Sea plate and locations of TVG, Taiwan and Mayon volcano; Canlaon volcano, Philippines. Night-Time 8-day average MODIS LSTs for the two active volcanoes were extracted and transformed by HHT; results are shown in Figure 9.

The most striking difference between the TVG and volcanoes of the Philippines is the deviation of the temperature data of the active volcanoes from the regular annual-cycle air temperature as shown in Figure 9(b,d). This confirms that the deviation of the annual-period component from regular annual-cycle air temperature records is a possible indicator for the restlessness of active volcanoes. Thus, we anticipate that the regular annual-period component from TVG's LST indicates it is currently quiet and resting.

A second observation is that short period components such as C1, C2 and C3 are more responsive to the volcano eruptions than the longer period components. C4 and C5 (inter-annual and quasi-biannual timescales) are only responsive to the eruptions of higher intensity as shown in Mayon volcano. This can be explained by the fact that

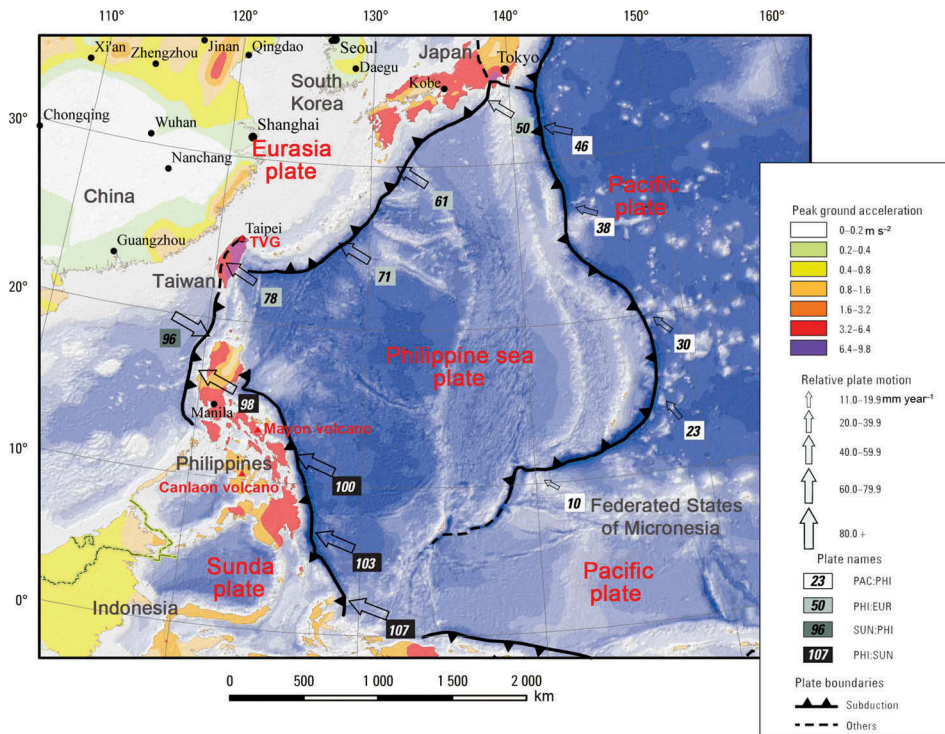


Figure 8. Seismic hazard and relative plate motion map in the Philippine Sea plate and vicinity (modified from Smoczyk et al. 2013). The Philippine Sea plate subducted to the west under the Eurasia plate at the Philippine Trench. Locations of TVG, Taiwan and Mayon volcano; Canlaon volcano, Philippines are indicated by red triangles.

longer period components such as C5–C8 have an amplitude 1 order lower than others (see Figure 5). These longer period oscillations generally reflect the fluctuation of longer term or bigger scale from the environment. In contrast, short-period components catch the variations of short term or local scale from the background.

Thirdly, the LST of craters increases with the eruptions in Mayon and Canlaon volcanoes. However, the high LST dependency of the eruptions is not persistent for all erupting events. One possible explanation is that high LST depends on the intensity and scale of each eruption, with the LST response being more overt. Another contributing factor, however, is that during the period of study, LST observations were missing prior to or following some eruption events. As a result of persistent cloud cover. In addition, the scale-mismatch effect should be accountable for the discrepancy between eruptions and high LST. For the dimension of volcanic craters (the crater size is measured by the mean diameter of the crater rim area) are generally less than 200 m, however, the pixel size of the MODIS LST products is 1 km.

Finally, the remote-sensing methods remain a number of limitations. Most importantly, sensors used for the infrared monitoring of volcanic activity is intrinsically restricted by the trade-off of temporal-spatial-spectral resolution. The trade-off between spatial, spectral and temporal resolution for imagery is a function of bandwidths on data transfer. Given a fixed bandwidth, a sensor with a high spectral resolution requires to lower either spatial or temporal resolution, and vice versa. These trade-offs are significant to the remote

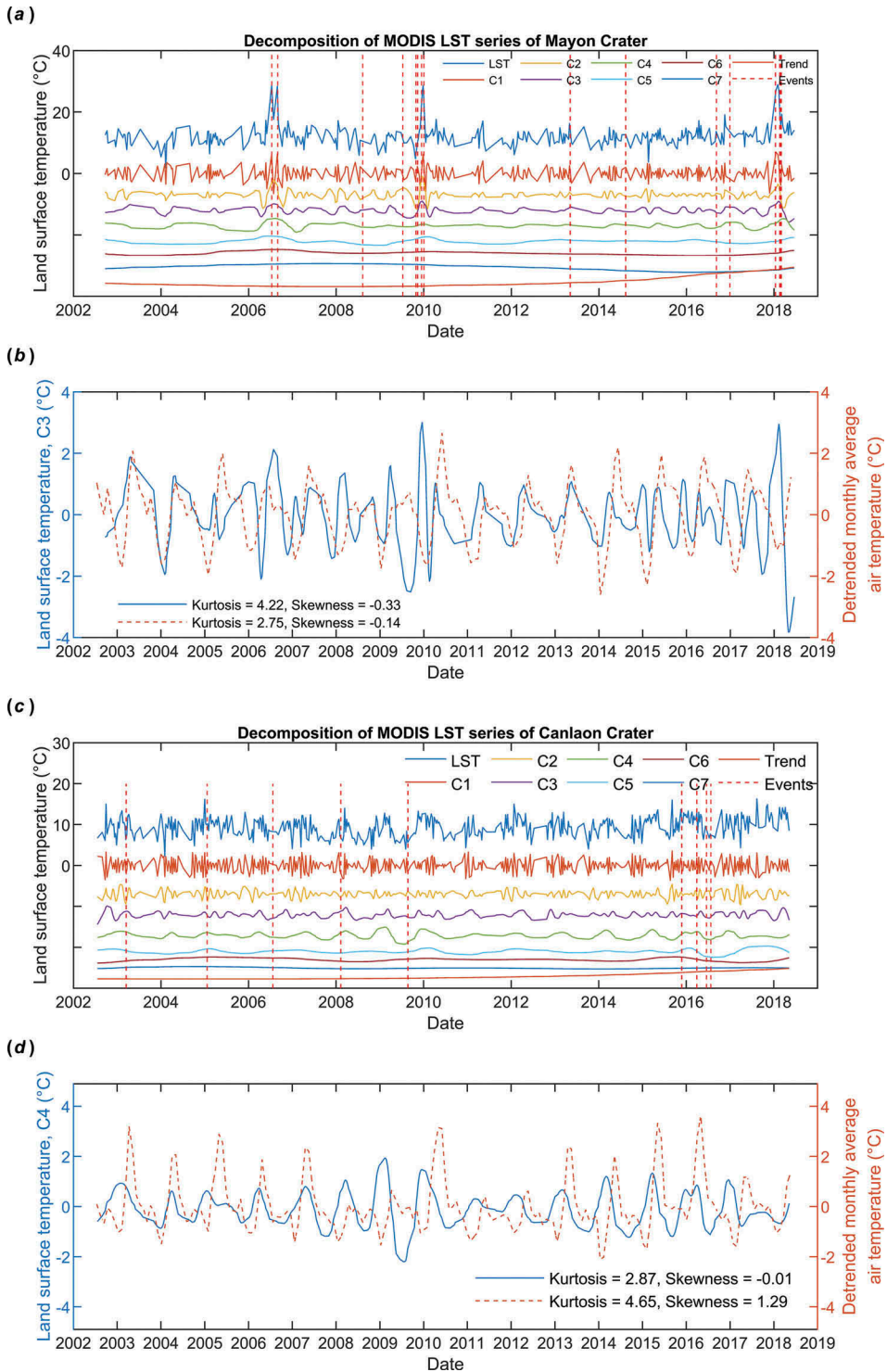


Figure 9. Decomposition of the MODIS LST at Mayon and Canlaon craters of Philippines. (a) HHT decomposed MODIS LST of Mayon crater from 2002–2018. The original MODIS LST is on the top plot, followed by the decomposed components C1–C7, and the trend is on the bottom plot. Recorded volcanic unrest and eruptions are indicated by dashed vertical red lines. (b) Comparison between the decomposed annual-cycle LST component 3 (C3) and the detrended monthly average air temperature at Mayon crater. (c) Same as panel (a) except for Canlaon crater. (d) Same as panel (b) except for LST component 4 (C4) at Canlaon crater.

monitoring of volcanic activity which fluctuates greatly in space, time and intensity. For example, in the case of prolonged eruption, the low spatial resolution (1-km) MODIS sensor is preferred for accurate observations, because its high temporal resolution (sub-daily) provides the timely monitoring of effusive activity. However, for the case of explosive eruption, the sub-daily temporal resolution imagery of MODIS sensor can be inadequate to record such events. Thus, despite its advantages of higher efficiency and larger regional scales, infrared remote sensing cannot be relied upon alone for volcanic monitoring.

4. Conclusions

This work aims to assess the eruptive potential of TVG by the satellite-derived LST monitoring-based approach. LST retrieved from the NASA Landsat 7 ETM+ thermal infrared imagery has been used to identify the Jinshan fault ROI as the target zone for further LST monitoring, and HHT has been used for analysing night-time 8-day average MODIS LST in Jinshan fault zone of TVG. Possible physical processes contributing to the HHT components (C1–C8) have been investigated. Specifically, the 370-day period component (about one year) is in line with the dominant period of original LST, which indicates seasonal variations in LST.

Comparison of LST annual oscillations with those of two active volcanoes in the Philippines shows that the annual-period component loses its regularity when an eruption occurs, meaning that the deviation of the annual-period component from annual-cycle air temperature is a possible indicator for volcanic activity. Consequently, the TVG's undistorted LST annual-period component implies its resting status and with no eruption potential for decades in the future.

The application of such a technique for the evaluation of volcanic activity is cost-and-time-effective. Compared with conventional in situ monitoring methods of point measurements established in TVO, remote-sensing methods that are advantaged by supplying reliable results which are spatially representative at larger regional scales. It is feasible that such a system could be integrated with existing volcanic monitoring systems to better understanding the potential activities in the TVG as well as volcanoes in other parts of the world.

Acknowledgements

The authors are thankful to the editor and reviewers for the careful and constructive comments. The Landsat 7 ETM+ imagery is available from <https://lpdaac.usgs.gov/>. The MODIS 8-day average LST products are from the Global 1 km level-3 MODIS Land Surface Temperature and Emissivity (LST/E) 8-day datasets (MYD11A2 Collection 6), available from <https://ladsweb.modaps.eosdis.nasa.gov/>. The air temperature products are from the NASA Prediction of Worldwide Energy Resource (POWER), available from <https://power.larc.nasa.gov/index.php>.

Disclosure statement

No potential conflict of interest was reported by the authors.

Funding

This research was funded by the Ministry of Science and Technology (MOST) of Taiwan, grant number MOST 106-2116-M-008-001 and MOST 107-2811-M-008-009.

ORCID

Hai-Po Chan  <http://orcid.org/0000-0002-6456-4273>

References

- Belousov, A., M. Belousova, C.-H. Chen, and G. F. Zellmer. 2010. "Deposits, Character and Timing of Recent Eruptions and Gravitational Collapses in Tatun Volcanic Group, Northern Taiwan: Hazard-related Issues." *Journal of Volcanology and Geothermal Research* 191 (3): 205–221. doi:10.1016/j.jvolgeores.2010.02.001.
- Blackett, M. 2013. "Review of the Utility of Infrared Remote Sensing for Detecting and Monitoring Volcanic Activity with the Case Study of Shortwave Infrared Data for Lascar Volcano from 2001–2005." *Geological Society, London, Special Publications* 380 (SP380): 10. doi:10.1144/SP380.10.
- Blackett, M. 2015. "An Initial Comparison of the Thermal Anomaly Detection Products of MODIS and VIIRS in Their Observation of Indonesian Volcanic Activity." *Remote Sensing of Environment* 171: 75–82. doi:10.1016/j.rse.2015.10.002.
- Blackett, M. 2017. "An Overview of Infrared Remote Sensing of Volcanic Activity." *Journal of Imaging* 3 (2): 13. doi:10.3390/jimaging3020013.
- Bull, K. F., C. Cameron, M. L. Coombs, A. Diefenbach, T. Lopez, S. McNutt, C. Neal, A. Payne, J. A. Power, and D. J. Schneider. 2012. *The 2009 Eruption of Redoubt Volcano, Alaska*. State of Alaska, Department of Natural Resources. doi: 10.1094/PDIS-11-11-0999-PDN
- Carn, S. A., L. Clarisse, and A. J. Prata. 2016. "Multi-decadal Satellite Measurements of Global Volcanic Degassing." *Journal of Volcanology and Geothermal Research* 311: 99–134. doi:10.1016/j.jvolgeores.2016.01.002.
- Chan, H.-P., and C.-P. Chang. 2018. "Exploring and Monitoring Geothermal and Volcanic Activity Using Satellite Thermal Infrared Data in TVG, Taiwan." *Terrestrial Atmospheric and Oceanic Sciences* 29: 1–18. doi:10.3319/TAO.2018.01.22.01.
- Chan, H.-P., C.-P. Chang, and P. D. Dao. 2018. "Geothermal Anomaly Mapping Using Landsat Etm+ Data in Ilan Plain, Northeastern Taiwan." *Pure and Applied Geophysics* 175: 303–323. doi:10.1007/s00024-017-1690-z
- Chang, C.-P., J.-Y. Yen, A. Hooper, F.-M. Chou, Y.-A. Chen, C.-S. Hou, W.-C. Hung, and M.-S. Lin. 2010. "Monitoring of Surface Deformation in Northern Taiwan Using DInSAR and PSInSAR Techniques." *Terrestrial, Atmospheric & Oceanic Sciences* 21: 3. doi:10.3319/TAO.2009.11.20.01(TH).
- Cheng, P. 1979. "Heat Transfer in Geothermal Systems." *Advances in Heat Transfer* 14: 1–105.
- Chu, C.-J., C.-T. Lee, and L. S. Teng. 1998a. "Structural Features and Quaternary Tectonics of the Chinshan Fault, Northern Taiwan." *Journal-geological Society of China-taiwan-* 41: 25–42.
- Chu, C.-J., C.-T. Lee, and L. S. Teng. 1998b. "Structural Features and Quaternary Tectonics of the Chinshan Fault, Northern Taiwan." *Journal of Geological Society of China (taiwan)* 41: 25–42.
- Delle Donne, D., A. J. L. Harris, M. Ripepe, and R. Wright. 2010. "Earthquake-induced Thermal Anomalies at Active Volcanoes." *Geology* 38 (9): 771–774. doi:10.1130/G30984.1.
- Divis, A. F. 1980. "The Petrology and Tectonics of Recent Volcanism in the Central Philippine Islands." *Washington DC American Geophysical Union Geophysical Monograph Series* 23: 127–144.
- Ewert, J. W., M. Guffanti, and T. L. Murray. 2005. *An assessment of volcanic threat and monitoring capabilities in the United States: framework for a National Volcano Early Warning System*.
- Flynn, L. P., A. J. L. Harris, and R. Wright. 2001. "Improved Identification of Volcanic Features Using Landsat 7 ETM+." *Remote Sensing of Environment* 78 (1–2): 180–193. doi:10.1016/S0034-4257(01)00258-9.

- Gupta, R. P. 2017. *Remote Sensing Geology*. Berlin: Springer.
- Hellman, M. J., and M. S. Ramsey. 2004. "Analysis of Hot Springs and Associated Deposits in Yellowstone National Park Using ASTER and AVIRIS Remote Sensing." *Journal of Volcanology and Geothermal Research* 135 (1–2): 195–219. doi:10.1016/j.jvolgeores.2003.12.012.
- Huang, N. E., and W. Zhaohua. 2008. "A Review on Hilbert-Huang Transform: Method and Its Applications to Geophysical Studies." *Reviews of Geophysics* 46: 2. doi:10.1029/2007RG000228.
- Huang, N. E., W. Zhaohua, J. E. Pinzón, C. L. Parkinson, S. R. Long, K. Blank, P. Gloersen, and X. Chen. 2009. "Reductions of Noise and Uncertainty in Annual Global Surface Temperature Anomaly Data." *Advances in Adaptive Data Analysis* 1 (03): 447–460. doi:10.1142/S1793536909000151.
- Huang, N. E., Z. Shen, S. R. Long, M. C. Wu, H. H. Shih, Q. Zheng, N.-C. Yen, C. C. Tung, and H. H. Liu. 1998. "The Empirical Mode Decomposition and the Hilbert Spectrum for Nonlinear and Non-stationary Time Series Analysis." Paper presented at the proceedings of the royal society of London A: mathematical, physical and engineering sciences. doi:10.1098/rspa.1998.0193
- Jyr-Ching, H., J. Angelier, J.-C. Lee, H.-T. Chu, and D. Byrne. 1996. "Kinematics of Convergence, Deformation and Stress Distribution in the Taiwan Collision Area: 2-D Finite-element Numerical Modelling." *Tectonophysics* 255 (3–4): 243–268. doi:10.1016/0040-1951(95)00140-9.
- Kereszturi, G., L. N. Schaefer, W. K. Schleiffarth, J. Procter, R. R. Pullanagari, S. Mead, and B. Kennedy. 2018. "Integrating Airborne Hyperspectral Imagery and LiDAR for Volcano Mapping and Monitoring through Image Classification." *International Journal of Applied Earth Observation and Geoinformation* 73: 323–339. doi:10.1016/j.jag.2018.07.006.
- Kim, K., C. Chang, K. Ma, J. Chiu, and K. Chen. 2005. "Modern Seismic Observations in the Tatun Volcano Region of Northern Taiwan: Seismic/volcanic Hazard Adjacent to the Taipei Metropolitan Area." *Terrestrial Atmospheric and Oceanic Sciences* 16 (3): 579. doi:10.3319/TAO.2005.16.3.579(T).
- Konstantinou, K. I., C. H. Lin, W. T. Liang, and Y. C. Chan. 2009. "Seismogenic Stress Field beneath the Tatun Volcano Group, Northern Taiwan." *Journal of Volcanology and Geothermal Research* 187 (3): 261–271. doi:10.1016/j.jvolgeores.2009.09.011.
- Konstantinou, K. I., C.-H. Lin, and W.-T. Liang. 2007. "Seismicity Characteristics of a Potentially Active Quaternary Volcano: The Tatun Volcano Group, Northern Taiwan." *Journal of Volcanology and Geothermal Research* 160 (3): 300–318. doi:10.1016/j.jvolgeores.2006.09.009.
- Lin, C.-H. 2016. "Evidence for a Magma Reservoir beneath the Taipei Metropolis of Taiwan from Both S-wave Shadows and P-wave Delays." *Scientific Reports* 6: 39500. doi:10.1038/srep39500
- Nunes, J.-C., and D. Eric. 2009. "Empirical Mode Decomposition: Applications on Signal and Image Processing." *Advances in Adaptive Data Analysis* 1 (01): 125–175. doi:10.1142/S1793536909000059.
- Nurmawati, A., and K. I. Konstantinou. 2018. "Hazard Assessment of Volcanic Ballistic Impacts at Mt Chihshin, Tatun Volcano Group, Northern Taiwan." *Natural Hazards* 92 (1): 77–92. doi:10.1007/s11069-018-3192-4.
- Pieri, D., and M. Abrams. 2004. "ASTER Watches the World's Volcanoes: A New Paradigm for Volcanological Observations from Orbit." *Journal of Volcanology and Geothermal Research* 135 (1–2): 13–28. doi:10.1016/j.jvolgeores.2003.12.018.
- Pyle, D. M., T. A. Mather, and J. Biggs. 2013. "Remote Sensing of Volcanoes and Volcanic Processes: Integrating Observation and Modelling—Introduction." *Geological Society, London, Special Publications* 380 (SP380): 14. doi:10.1144/SP380.14.
- Queißer, M., M. Burton, and R. Kazahaya. 2018. "Insights into Geological Processes with CO2 Remote sensing—A Review of Technology and Applications." *Earth-science Reviews* 188:389–426. doi:10.1016/j.earscirev.2018.11.016
- Ramsey, M. S., and A. J. L. Harris. 2013. "Volcanology 2020: How Will Thermal Remote Sensing of Volcanic Surface Activity Evolve over the Next Decade?" *Journal of Volcanology and Geothermal Research* 249: 217–233. doi:10.1016/j.jvolgeores.2012.05.011.
- Ramsey, M. S., A. J. L. Harris, and D. A. Crown. 2016. "What Can Thermal Infrared Remote Sensing of Terrestrial Volcanoes Tell Us about Processes past and Present on Mars?" *Journal of Volcanology and Geothermal Research* 311: 198–216. doi:10.1016/j.jvolgeores.2016.01.012.
- Roberti, G., B. Ward, B. van Wyk de Vries, P. Friele, L. Perotti, J. J. Clague, and M. Giardino. 2018. "Precursory Slope Distress Prior to the 2010 Mount Meager Landslide, British Columbia." *Landslides* 15 (4): 637–647. doi:10.1007/s10346-017-0901-0.

- Smoczyk, G. M., G. P. Hayes, M. W. Hamburger, H. M. Benz, A. Villaseñor, and K. P. Furlong. 2013. *Seismicity of the Earth 1900–2012 Philippine Sea Plate and Vicinity*. US Geological Survey. Open-File Report 2010-1083-M. doi:[10.3133/ofr20101083M](https://doi.org/10.3133/ofr20101083M)
- Song, S.-R., S. H. U. J. O. N. G. Tsao, and H. U. A. N. N.-J. I. H. Lo. 2000. "Characteristics of the Tatun Volcanic Eruptions, North Taiwan: Implications for a Cauldron Formation and Volcanic Evolution." *Journal of the Geological Society of China (taiwan)* 43 (2): 361–377.
- Song, S.-R., T.-M. Chen, S. Tsao, H.-F. Chen, and H.-C. Liu. 2007. "Lahars in and around the Taipei Basin: Implications for the Activity of the Shanchiao Fault." *Journal of Asian Earth Sciences* 31 (3): 277–286. doi:[10.1016/j.jseae.2006.07.017](https://doi.org/10.1016/j.jseae.2006.07.017).
- Spinetti, C., V. Carrère, M. Fabrizia Buongiorno, A. Jefferson Sutton, and T. Elias. 2008. "Carbon Dioxide of PuuOo Volcanic Plume at Kilauea Retrieved by AVIRIS Hyperspectral Data." *Remote Sensing of Environment* 112 (6): 3192–3199. doi:[10.1016/j.rse.2008.03.010](https://doi.org/10.1016/j.rse.2008.03.010).
- Steffke, A. M., and A. J. L. Harris. 2011. "A review of algorithms for detecting volcanic hot spots in satellite infrared data." *Bulletin of Volcanology* 73 (9): 1109–1137. doi:[10.1007/s00445-011-0487-7](https://doi.org/10.1007/s00445-011-0487-7).
- Teng, L. S., C. T. Lee, C.-H. I.-H.-H. S. I. U. N. G. Peng, W. F. Chen, and C. J. Chu. 2001. "Origin and Geological Evolution of the Taipei Basin, Northern Taiwan." *Western Pacific Earth Sciences* 1 (2): 115–142.
- Tsai, Y.-W., S.-R. Song, H.-F. Chen, L. Shu-Fen, L. Ching-Hua, L. Wei, and S. Tsao. 2010. "Volcanic Stratigraphy and Potential Hazards of the Chihsingshan Volcano Subgroup in the Tatun Volcano Group, Northern Taiwan." *Terrestrial, Atmospheric & Oceanic Sciences* 21: 3. doi:[10.3319/TAO.2010.02.22.03](https://doi.org/10.3319/TAO.2010.02.22.03)(TH).
- Wan, Z. 2014. "New Refinements and Validation of the Collection-6 MODIS Land-surface Temperature/emissivity Product." *Remote Sensing of Environment* 140: 36–45. doi:[10.1016/j.rse.2013.08.027](https://doi.org/10.1016/j.rse.2013.08.027).
- Wan, Z., and L. Zhao-Liang. 1997. "A Physics-based Algorithm for Retrieving Land-surface Emissivity and Temperature from EOS/MODIS Data." *IEEE Transactions on Geoscience and Remote Sensing* 35 (4): 980–996. doi:[10.1109/36.602541](https://doi.org/10.1109/36.602541).
- Wang, J.-C., J.-H. Wang, C.-F. Shieh, and Y.-H. Yeh. 2010. "Static Stress Transfer between the Chinshan and Shanchiao Faults in the Taipei Metropolitan Area." *Terrestrial, Atmospheric & Oceanic Sciences* 21: 3. doi:[10.3319/TAO.2009.11.24.01](https://doi.org/10.3319/TAO.2009.11.24.01)(TH).
- Wang, J.-H. 2008. "Potential Earthquakes Rupturing the Chinshan and Shangjiao Faults in the Taipei Metropolitan Area." *Terrestrial, Atmospheric & Oceanic Sciences* 19: 3. doi:[10.3319/TAO.2008.19.3.205](https://doi.org/10.3319/TAO.2008.19.3.205)(T).
- Wang, Y.-H., C.-H. Yeh, H.-W. V. Young, K. Hu, and M.-T. Lo. 2014. "On the Computational Complexity of the Empirical Mode Decomposition Algorithm." *Physica A: Statistical Mechanics and Its Applications* 400: 159–167. doi:[10.1016/j.physa.2014.01.020](https://doi.org/10.1016/j.physa.2014.01.020).
- Webley, P. W., D. Atkinson, R. L. Collins, K. Dean, J. Fochesatto, K. Sassen, C. F. Cahill, A. Prata, C. J. Flynn, and K. Mizutani. 2008. "Predicting and Validating the Tracking of a Volcanic Ash Cloud during the 2006 Eruption of Mt. Augustine Volcano." *Bulletin of the American Meteorological Society* 89 (11): 1647–1658. doi:[10.1175/2008BAMS2579.1](https://doi.org/10.1175/2008BAMS2579.1).
- Wooster, M., G. Roberts, A. Smith, J. Johnston, P. Freeborn, S. Amici, and A. Hudak. 2013. "Thermal infrared remote sensing: sensors, methods, applications."
- Wright, R., L. Flynn, H. Garbeil, A. Harris, and E. Pilger. 2002. "Automated Volcanic Eruption Detection Using MODIS." *Remote Sensing of Environment* 82 (1): 135–155. doi:[10.1016/S0034-4257\(02\)00030-5](https://doi.org/10.1016/S0034-4257(02)00030-5).
- Yang, C. C., J. K. Liu, M. T. Huank, and W. S. Chen. 2004. "DTM for Mapping the Volcanic Landforms of Tatun Volcano Group in Northern Taiwan." *Journal of Photogrammetry and Remote Sensing* 9 (2): 1–8.
- Yang, T. F., Y. Sano, and S. R. Song. 1999. "3He/4He Ratios of Fumaroles and Bubbling Gases of Hot Springs in Tatun Volcano Group, North Taiwan." *Nuovo Cimento-societa Italiana Di Fisica Sezione C* 22: 281–286.
- Zhao, C., B. E. Hobbs, and A. Ord. 2008. *Convective and Advective Heat Transfer in Geological Systems*. Berlin: Springer.